

**Evolving impacts of multi-year La Niña events on atmospheric circulation and US drought**

Yuko M. Okumura<sup>1</sup>, Pedro DiNezio<sup>1</sup>, and Clara Deser<sup>2</sup>

<sup>1</sup> Institute for Geophysics, Jackson School of Geosciences, University of Texas at Austin

<sup>2</sup> Climate and Global Dynamics Laboratory, National Center for Atmospheric Research

**Contents of this file**

Text S1

Figures S1 to S12

**Introduction**

This Supplementary Information contains 1 text and 12 figures to complement the observational composite analysis of multi-year La Niña teleconnections presented in the main text. In particular, the robustness of observational composite analysis is examined in Figures S3, S4, S6, and S7, and the observational composite analysis is compared with atmospheric model simulations described in Text S1 in Figures S7 and S9-11. We also present the time series of Niño-3.4 index used to define multi-year La Niña events (Figures S1 and S2), observational composite analysis for the NH warm season (Figure S5), polar stereographic maps of cold season atmospheric circulation anomalies based on observational composite (Figure S8), and observed atmospheric anomaly pattern associated with the first SVD mode of cold season tropical Pacific SST and North Pacific atmospheric circulation (Figure S12).

**Text S1**

The observational composite analysis of multi-year La Niña teleconnections is compared with atmospheric model simulations forced with observed SSTs. We use the CAM version 5 [Hurrell *et al.*, 2013] at nominal 1° horizontal resolution and conduct a 60-member ensemble simulation forced with monthly global SSTs composited for year -1 through 3 of 8 multi-year La Niña events during 1948-2013 (referred to as LN2 run). The ensemble mean response is compared with monthly climatologies of a 50-year control simulation forced with monthly climatological SSTs for the same period. We also analyze 3 ensemble simulations forced with observed monthly global SSTs (referred to as GOGA runs) using the CAM5 (10 members for 1880-2015) and CAM4 (5 members for 1900-2011) and the GFDL AM2.1 (10 members for 1870-2004) [Li *et al.*, 2010]. Further information and data of the CAM GOGA runs are available through the Climate Variability and Change Working Group of the Climate Earth System Model ([http://www.cesm.ucar.edu/working\\_groups/CVC/](http://www.cesm.ucar.edu/working_groups/CVC/)). The ensemble mean anomalies from these GOGA runs are detrended and composited in the same manner as for the observational analysis. For the CAM GOGA runs, we also conduct composite analysis for individual ensemble members. (Individual ensemble members are not available for the AM2.1 GOGA run.) The SST forcing is based on a merged product of the HadISST and OISST [Hurrell *et al.*, 2008] in all the simulations except the CAM5 GOGA run, which is forced with the Extended Reconstructed SST (ERSST) version 4 [Huang *et al.*, 2015].

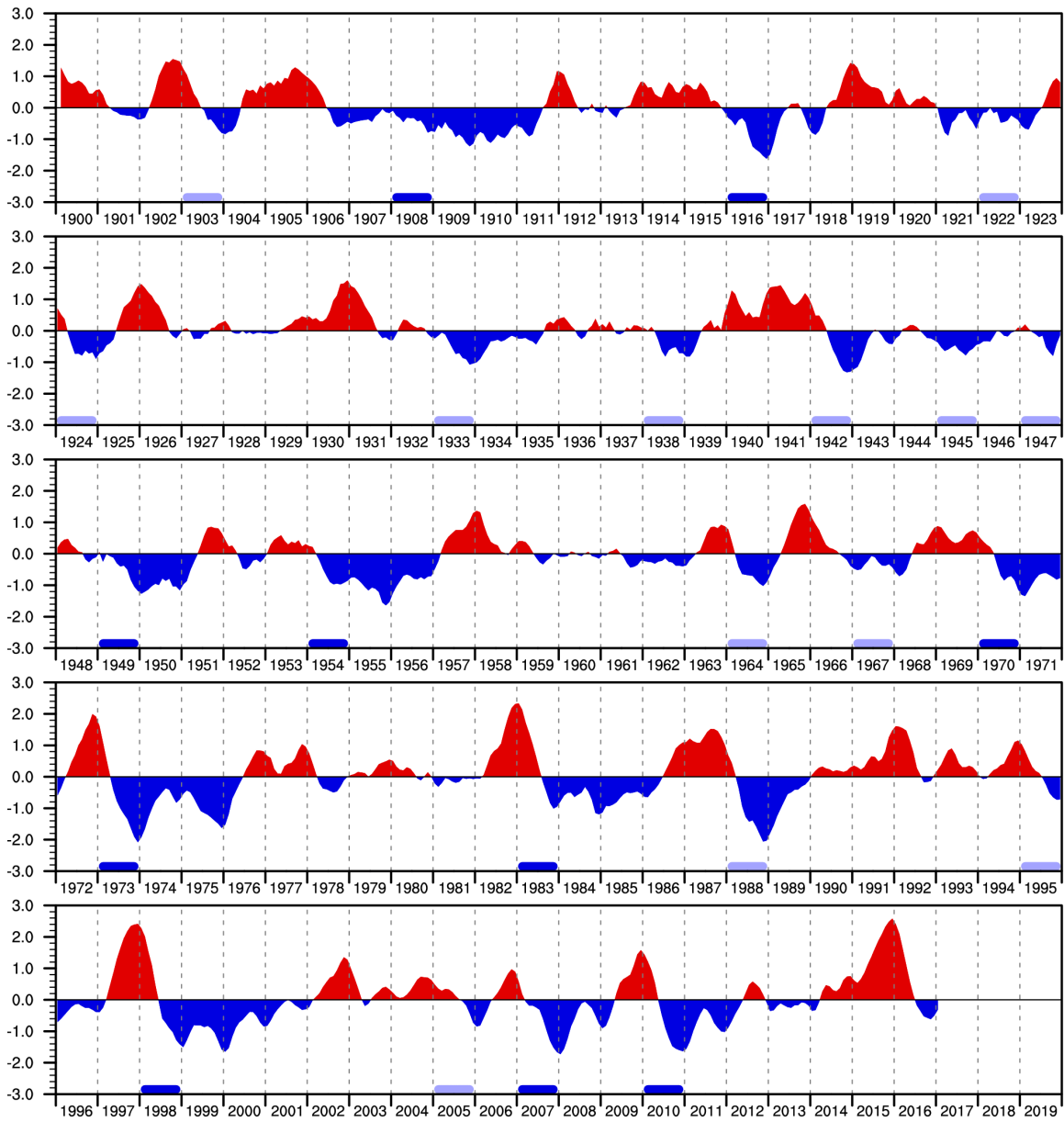


**Figure S1.** Time series of the Niño-3.4 index (°C) based on the HadISST dataset for 1900-2016. Year 0 of multi-year (single-year) La Niña events are indicated by thick horizontal blue (light blue) bars. A multi-year (single-year) La Niña event is identified when the Niño-3.4 index falls below  $-0.75$  standard deviations in any month during Oct(0)-Feb(1), and is below (above)  $-0.5$  standard deviations in any month (all months) during Oct(1)-Feb(2). There are 10 (13) multi-year (single-year) La Niña events for this period.

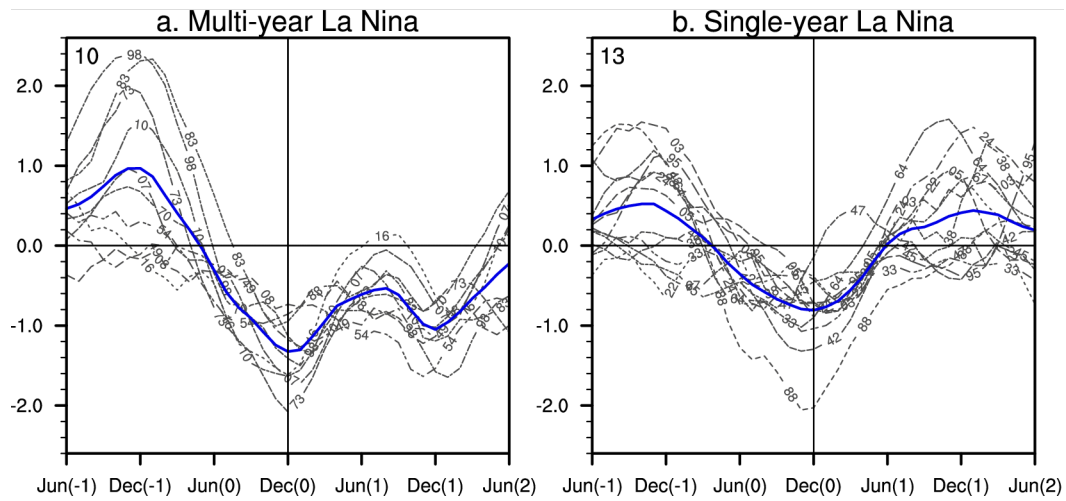


**Figure S2.** Time series of the Niño-3.4 index ( $^{\circ}\text{C}$ ) overlaid from Jun(-1) to Jun(2) for (a) multi-year and (b) single-year La Niña events based on the HadISST dataset for 1900-2016. Thick blue curves are composite time series. The last two digits of year 0 are indicated on curves for individual events.

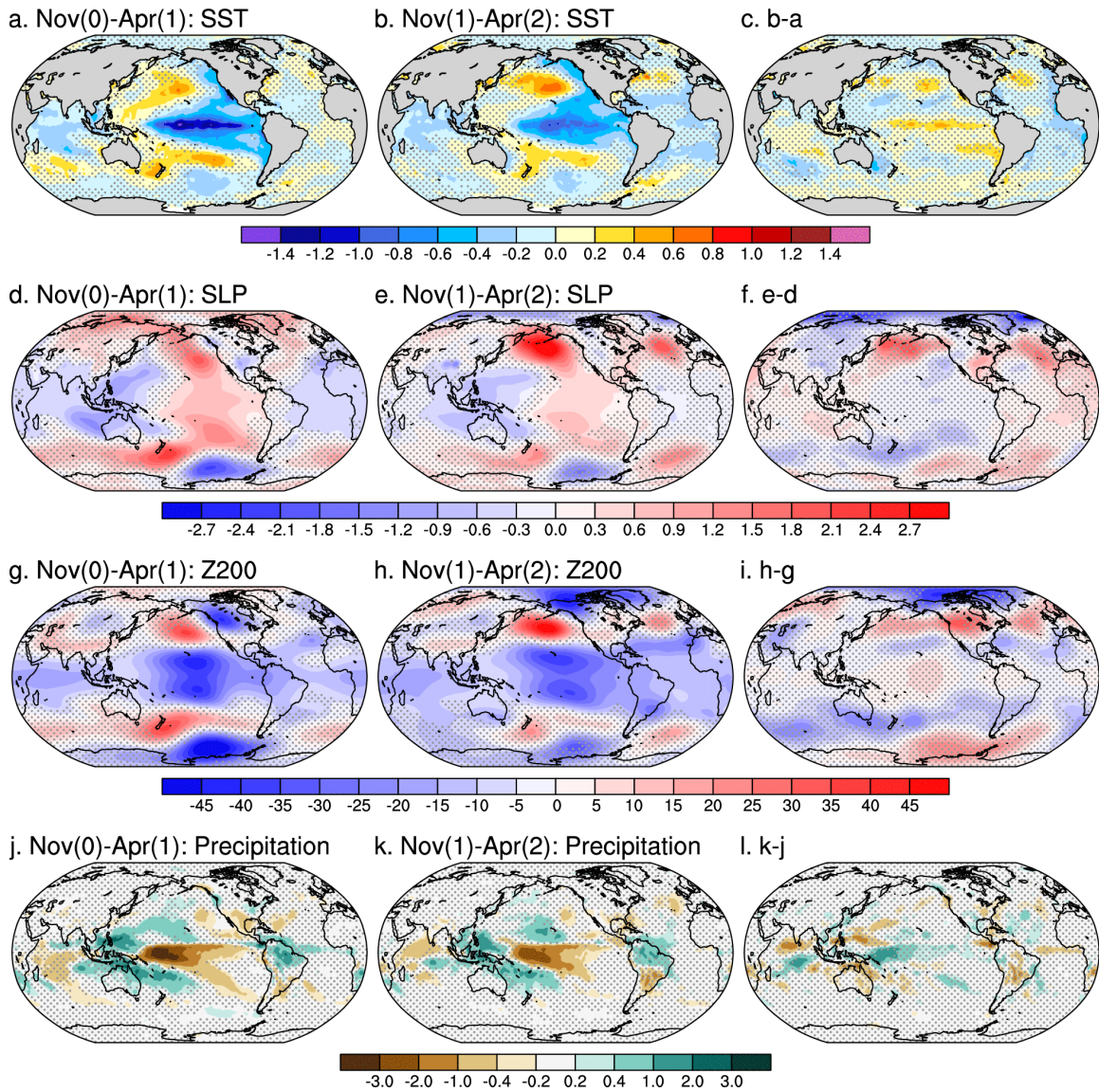


**Figure S3.** Observed ocean-atmosphere anomalies during the first and second cold seasons of a composite multi-year La Niña event and their statistical significance. (a-c) SST ( $^{\circ}\text{C}$ ), (d-f) SLP (hPa), (g-i) Z200 (m), and (j-l) precipitation ( $\text{mm day}^{-1}$ ) anomalies over the global domain for (a, d, g, and j) Nov(0)-Apr(1), (b, e, h, and k) Nov(1)-Apr(2), and (c, f, i, and l) their difference (the second minus the first year). The anomalies that are not statistically significant at the 90% confidence level are masked with gray stippling. Based on the HadISST and 20CR datasets for 1901-2012.

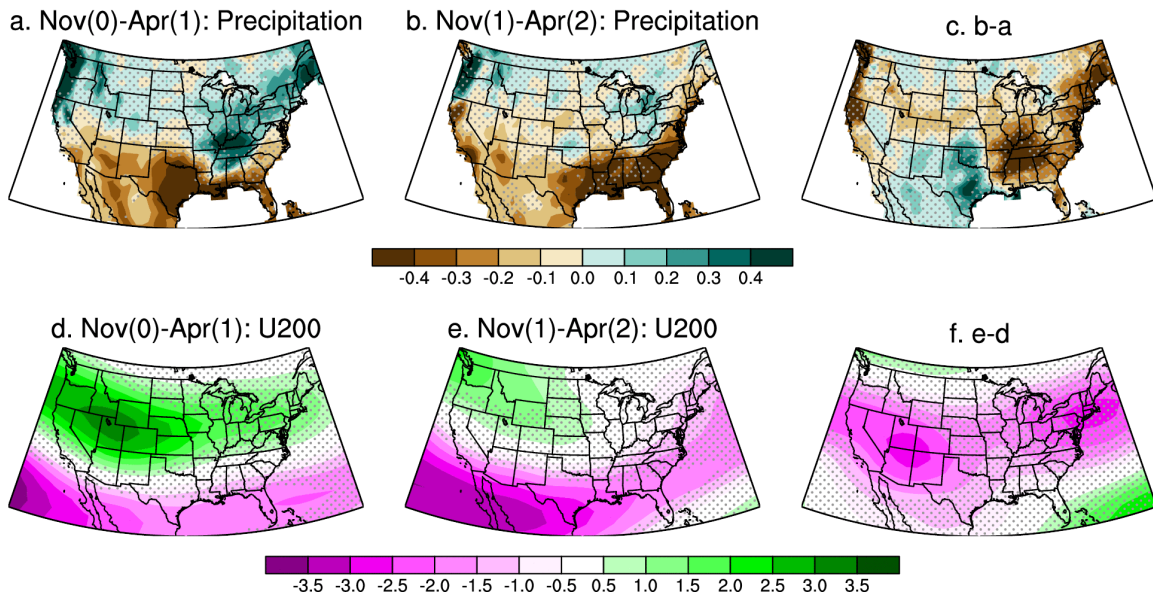


**Figure S4.** Same as in Figure S3 but for (a-c) terrestrial precipitation ( $\text{mm day}^{-1}$ ) and (d-f) U200 ( $\text{m s}^{-1}$ ) over the US based on the GPCP and 20CR datasets.

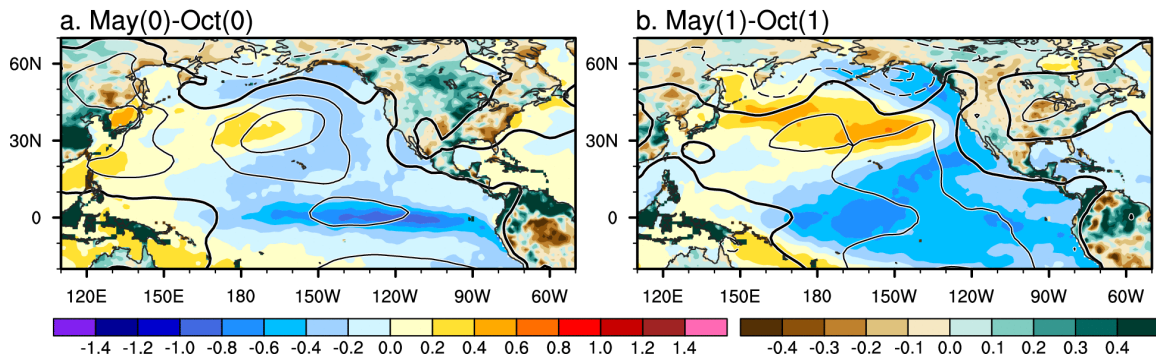


**Figure S5.** Observed ocean-atmosphere anomaly patterns during the first and second warm seasons of a composite multi-year La Niña event. SST (shading over the ocean, °C), terrestrial precipitation (shading over land,  $\text{mm day}^{-1}$ ), and SLP (contours at intervals of 0.5 hPa) anomalies over the Pacific-North American sector for (a) May(0)-Oct(0) and (b) May(1)-Oct(1). Based on the HadISST, GPCP, and 20CR datasets for 1901-2012.

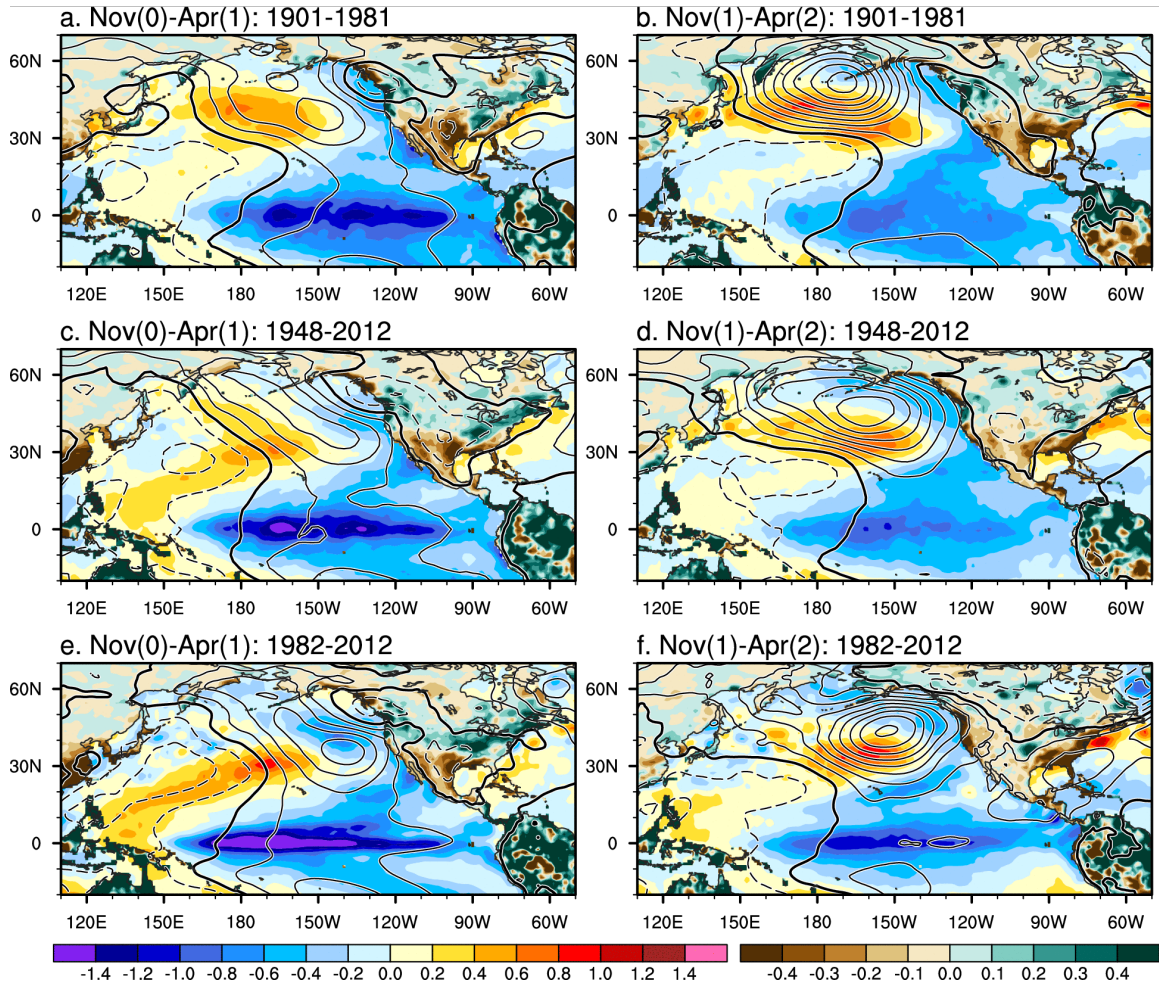


**Figure S6.** Observed ocean-atmosphere anomaly patterns during the first and second cold seasons of a composite multi-year La Niña event. SST (shading over the ocean, °C), terrestrial precipitation (shading over land, mm day<sup>-1</sup>), and SLP (contours at intervals of 0.5 hPa) anomalies over the Pacific-North American sector for (a, c, and e) Nov(0)-Apr(1) and (b, d, and f) Nov(1)-Apr(2). Based on (a and b) the HadISST, GPCC, and 20CR datasets for 1901-1981, (c and d) the HadISST, GPCC, and NCEP-NCAR reanalysis datasets for 1948-2012, and (e and f) the OISST, GPCC, and ERA-Interim datasets for 1982-2012.

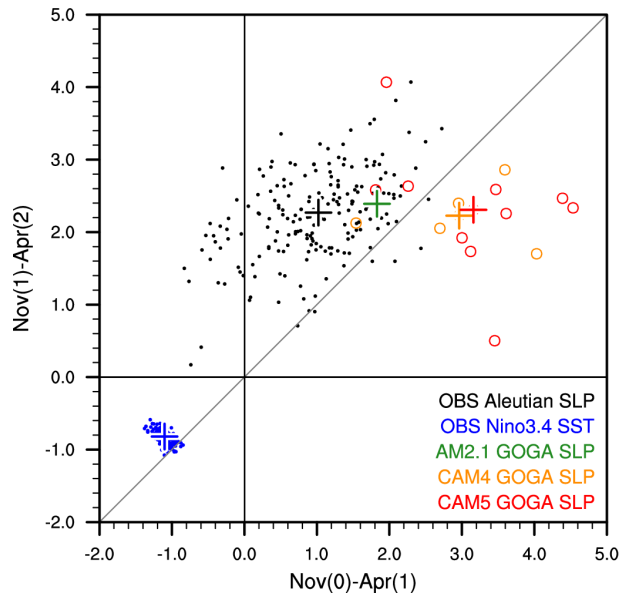


**Figure S7.** Scatterplot of ocean-atmosphere anomalies for the first and second cold seasons (Nov-Apr) of a composite multi-year La Niña event. Black and blue dots show composites of the Aleutian low SLP ( $40^{\circ}$ - $60^{\circ}$ N,  $170^{\circ}$ E- $140^{\circ}$ W; hPa) and Niño-3.4 SST ( $^{\circ}$ C) indices, respectively, for 200 randomly selected bootstrapped samples of 10 multi-year La Niña events based on the 20CR and HadISST datasets for 1901-2012 (see *Deser et al.* [2017] for methods). Orange and Red circles are composites of the Aleutian low SLP index for individual members of the CAM4 and CAM5 GOGA runs, respectively. Crosses show ensemble mean values in corresponding colors. Ensemble mean composite of the Aleutian low SLP index is also shown for the AM2.1 GOGA run in green. Gray line indicates where the first and second year values are equal. In most observational composites and AM2.1, the Aleutian low response is larger in the second than the first year despite weaker tropical SST forcing. The majority of CAM4 and 5 ensemble members are outside the range of observational uncertainty and the Aleutian low response weakens from the first to the second year.

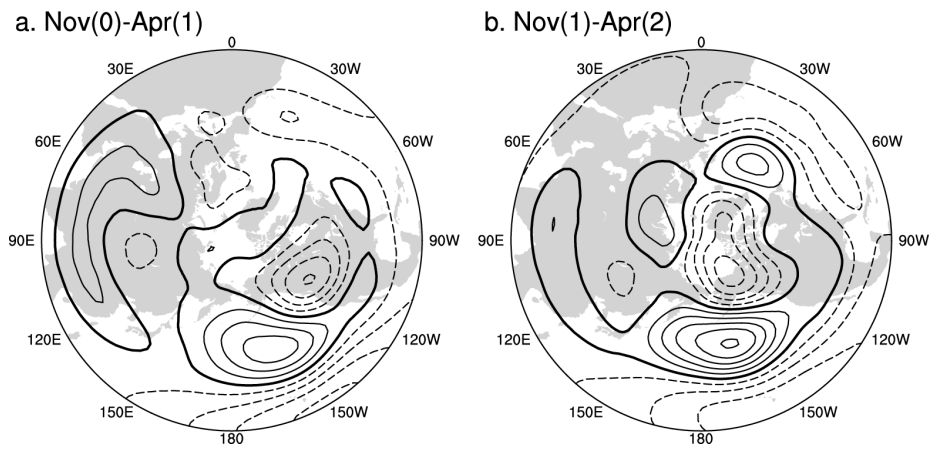


**Figure S8.** Observed Z200 anomaly patterns during the first and second cold seasons of a composite multi-year La Niña event. Z200 anomalies (contours at intervals of 10 m) over the NH (poleward of 15°N) for (a) Nov(0)-Apr(1) and (b) Nov(1)-Apr(2). Based on the 20CR dataset for 1901-2012.

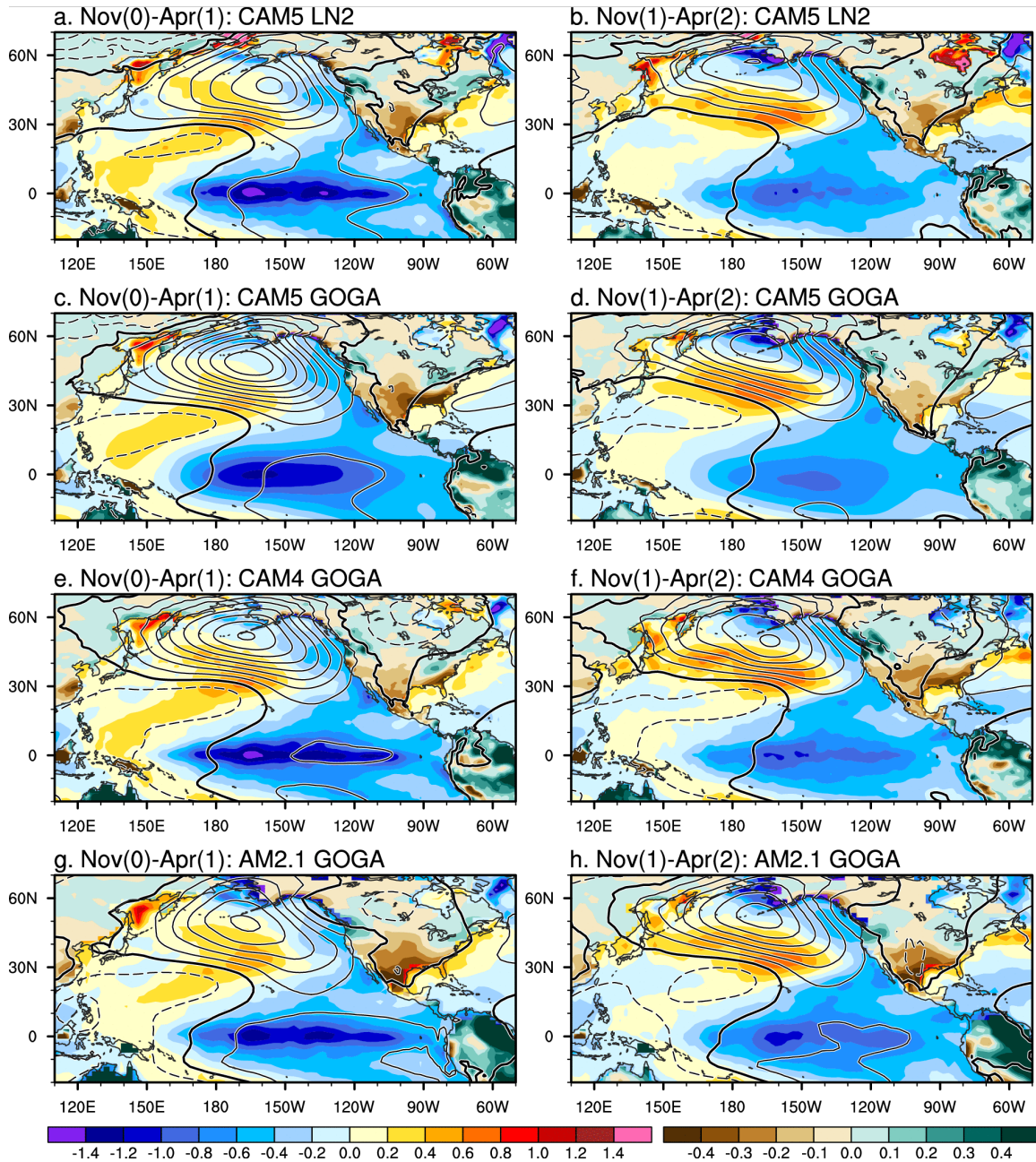


**Figure S9.** Ocean-atmosphere anomaly patterns during the first and second cold seasons of a composite multi-year La Niña event based on the atmospheric model simulations. Prescribed SST forcing (shading over the ocean, °C) and ensemble-mean terrestrial precipitation (shading over land, mm day<sup>-1</sup>) and SLP (contours at intervals of 0.5 hPa) response over the Pacific-North American sector for (a, c, e, and g) Nov(0)-Apr(1) and (b, d, f, and h) Nov(1)-Apr(2). Based on (a and b) the CAM5 LN2 run and (c and d) the CAM5, (e and f) CAM4, and (g and h) AM2.1 GOGA runs. Note that the sharp equatorial cooling in the first year is not captured well in the SST forcing used in the CAM5 GOGA run (ERSST).

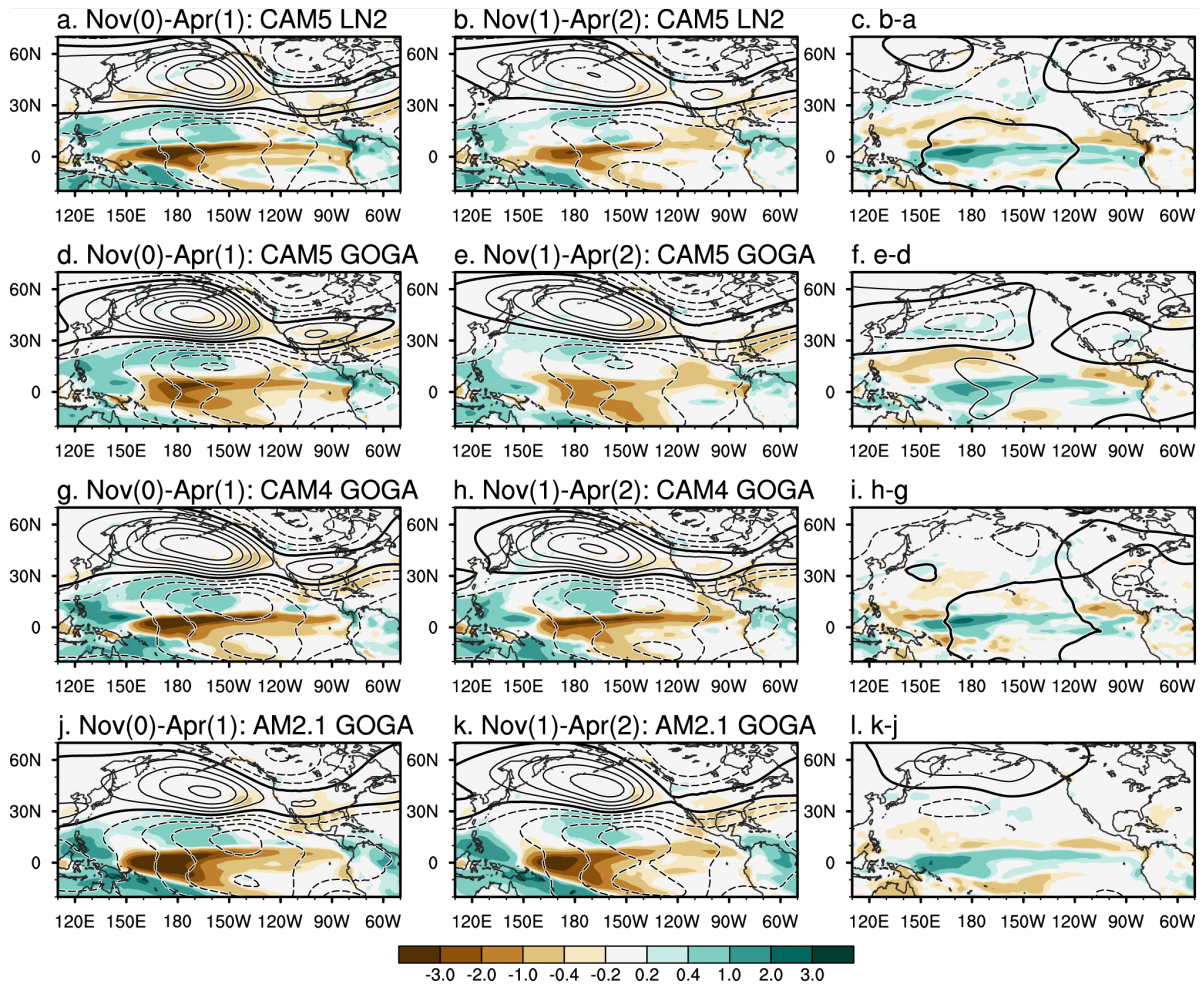


**Figure S10.** Atmospheric anomaly patterns during the first and second cold seasons of a composite multi-year La Niña event based on the atmospheric model simulations. Ensemble-mean precipitation (shading,  $\text{mm day}^{-1}$ ) and Z200 (contours at intervals of 10 m) response over the Pacific-North American sector for (a, d, g, and j) Nov(0)-Apr(1), (b, e, h, and k) Nov(1)-Apr(2), and (c, f, i, and l) their difference (the second minus the first year). Based on (a-c) the CAM5 LN2 run and (d-f) the CAM5, (g-i) CAM4, and (j-l) AM2.1 GOGA runs.

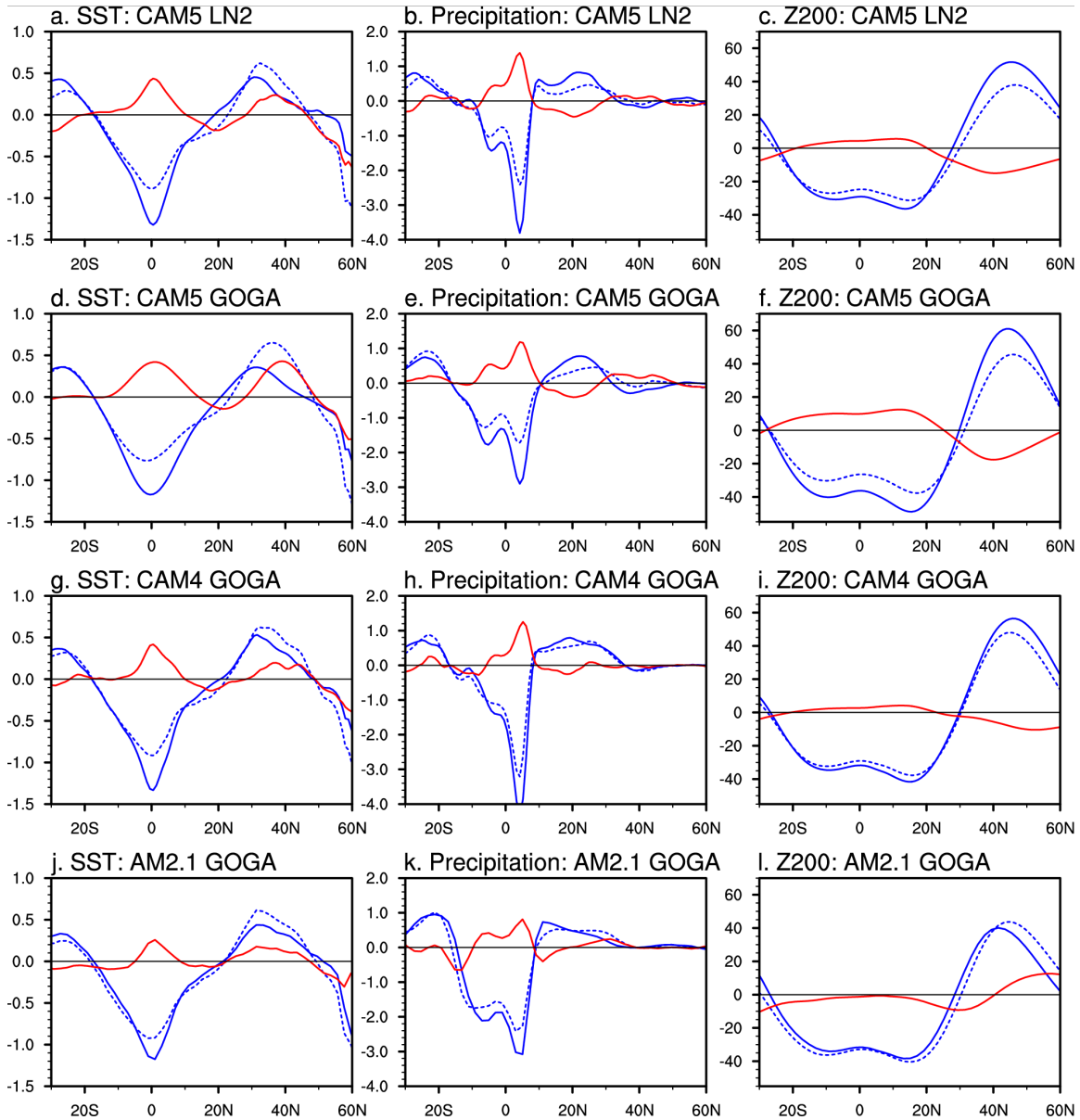


**Figure S11.** Meridional profiles of ocean-atmosphere anomalies in the central Pacific (150°W-180°) during the first and second cold seasons of a composite multi-year La Niña event based on the atmospheric model simulations. (a, d, g, and j) Prescribed SST forcing (°C) and ensemble-mean (b, e, h, and k) precipitation (mm day<sup>-1</sup>) and (c, f, i, and l) Z200 (m) response for Nov(0)-Apr(1) (blue solid), Nov(1)-Apr(2) (blue dashed), and their difference (the second minus the first year; red). Based on (a-c) the CAM5 LN2 run and (d-f) the CAM5, (g-i) CAM4, and (j-l) AM2.1 GOGA runs. Note that the sharp equatorial cooling in the first year is not captured well in the SST forcing used in the CAM5 GOGA run (ERSST).

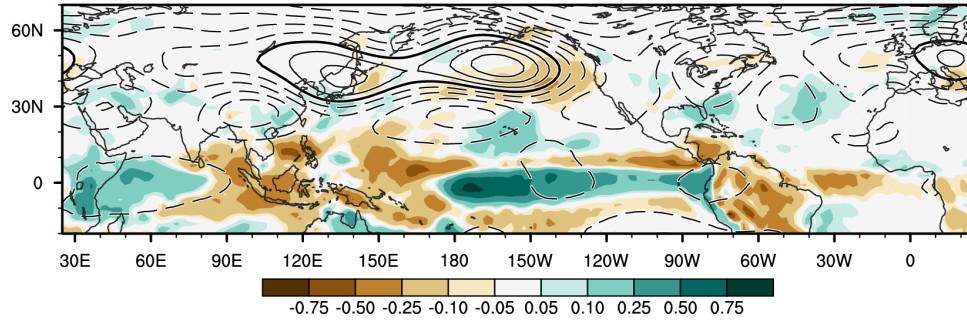


**Figure S12.** Observed atmospheric anomaly pattern associated with the first SVD mode of cold season tropical Pacific SST (20°S-20°N, 140°E-80°W) and North Pacific Z200 (10°-70°N, 130°E-70°W) anomalies. Regression map of precipitation (shading, mm day<sup>-1</sup>) and Z200 (contours at intervals of 2.5 m) based on the standardized SST expansion coefficient. Linear regressions on the Niño-3.4 index are removed from all fields prior to the analysis. Based on the HadISST and 20CR datasets for 1900-2012.